International Journal of Trend in Scientific Research and Development (IJTSRD)
Volume 6 Issue 5, July-August 2022 Available Online: www.ijtsrd.com e-ISSN: 2456 – 6470

Comparative Study of the Tribological Properties of the Swashplate Axial Piston Pump for Different Materials of the Valve Plate on Different Load Applications

Andrews Larbi*[1], Philip Adu Sarfo[2], Zorobabel Vubu Phuati[3]

[1]School of Material Science and Engineering, Zhengzhou University, Zhengzhou, Henan, China
[2]School of Management Engineering, Zhengzhou University, Zhengzhou, Henan, China
[3]College of Engineering, Zhejiang Normal University, Jinhua, Zhejiang, China

ABSTRACT

For swashplate-type axial piston machines, one of the most important parts is the lubricating interface between the valve plate and the cylinder block. When the valve plate and cylinder are subjected to pulsating loads, the interface between the two serves as a bearing and a seal. However, at the low speed of the pump, insufficient lubrication of the contact causes quick wear and substantial friction loss, drastically decreasing the pump's efficiency. Therefore, the material composition for fabricating the friction pair could contribute to the pump's efficiency. In this paper, an accurate prediction of the time-dependent tribological interface characteristics was performed to instruct the interface design efficiently and load holding capacity. Ball-on-disc tests were conducted to investigate the friction and wear behaviors of the valve plate/cylinder block interface using three types of valve plate materials. Cr12Mov base bronze coating (S1) prepared by physical vapor deposition has better tribological performance than the other two specimens of 38CrMoAl base bronze coating (S2) prepared by chemical vapor deposition and ductile Iron (S3). Results indicate that the S2 valve plate showed a much lower friction coefficient and wear rate. The scratch comparison reveals that the S2 specimen enhances the desired fracture toughness and protects the coatings from severe wear. S3 specimen has the lowest wear rate for the disc but higher friction coefficients and causes severe wear to its counter body surface (B4) due to differences in material composition and hardness.

KEYWORDS: *Friction; Wear; Axial piston pump; Valve plate; Cylinder block*

How to cite this paper: Andrews Larbi | Philip Adu Sarfo | Zorobabel Vubu Phuati "Comparative Study of the Tribological Properties of the Swashplate Axial Piston Pump for Different Materials of the Valve Plate on Different Load Applications" Published in International Journal of Trend in Scientific Research and Development (ijtsrd), ISSN: 2456-6470, Volume-6 | Issue-5, August 2022, pp.1703-1713, URL: www.ijtsrd.com/papers/ijtsrd51730.pdf

IJTSRD51730

1. INTRODUCTION

The principle of the hydraulic transfer of energy can be found in many industrial ranges of applications. Due to the high achievement density, the compact building method, and the small efficiency weight, hydraulic drives are of great importance for use in the mobile range. Under the rotation drives, the axial piston machine in swashplate design belongs to the preferential construction principles due to its compact and durable building method, which gets along with comparatively few construction units [1]， [2]. The further advantages of the swashplate axial piston pump, in particular, are compact and can operate at high pressure and high overall efficiency [3], [4], [5]. Because axial piston pumps usually operate under severe conditions, the tribological parts are crucial [6]. The valve and cylinder block interface is essential in an axial piston pump as these two elements generate most of the frictional loss in the pump [7]. In particular, the low-speed friction characteristics of the internal pump parts come into serious question, as they are subject to mixed lubrication, which leads to increased friction loss and a higher wear rate [8]. Fig. 1. Shows the swashplate axial piston hydraulic pump with multiple pistons arranged within the rotating kit on a given pitch radius around the main pump shaft. The pistons are encased by a cylinder block connected

to the main pump shaft, often through a mechanical spline [9]. The pressing force, the spring force, and the separating force between the valve plate/cylinder block are all determined by the oil film pressure and can be obtained numerically and experimentally, which has also been reported in previous works [10], [11],[12].

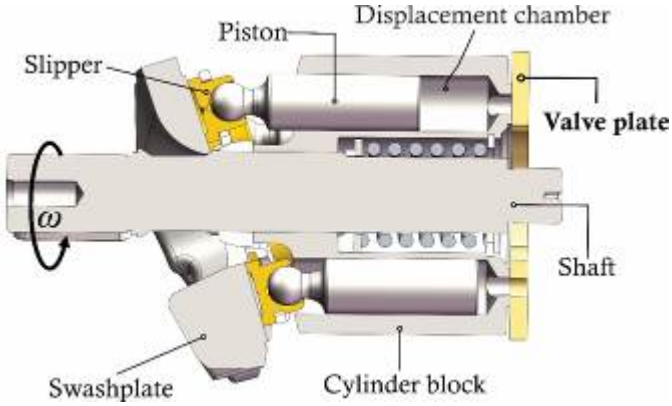

Fig. 1 A schematic of the swashplate type axial piston pump

Recently, low-speed efficiency due to insufficient lubrication has drawn considerable attention. The contact between the valve plate and cylinder block is crucial because the mechanical efficiency of the whole pump depends heavily on these two components, particularly at low speeds. Michael et al. [13] investigated the problem by examining the hydraulic fluids. They concluded that formulating a fluid with low static boundary friction coefficients and the minor changes in viscosity at increased temperature and pressure could improve start-up efficiency. Lee et al. [10] reported their achievements by applying coatings to improve the low-speed efficiency of a piston pump. Results showed that by representing the improvement in the torque efficiency of the whole pump based upon the degree of the friction coefficient reduction, CrZrN coatings exhibited approximately a 0.35% higher improvement at 300 bar and 100 rpm than CrSiN coatings and the low-speed efficiency increased considerably [14].

More so, research on surface morphology and topography has already improved many industrial applications, such as bearings [15] and gears [16],[17]. However, the comparative studies of surface morphology for different materials of the valve plate of swashplate type axial piston pump have not yet been systematically investigated from a tribology perspective.

A layer of oil film exists between the valve plated and cylinder block in ideal conditions, which lubricates the action of the friction pair [18]. However, because the sealing strips separate the higher-pressure area of the outlet from the lower pressure area of the inlet, a periodic eccentric moment occurs in the valve plate, causing an imbalance between the downward compressive stress and the upward support. The cylinder block will then come into touch with a portion of the valve plate, causing wear and tear [19]. The pressure distribution on a valve plate varies depending on the valve plate geometry and working pressure. Wang et al. [20] numerically calculated the pressure distribution of a valve plate with oil outlet pressure at 25 MPa. He found that the pressure ranged from 2 MPa to 25 MPa on the suction port of the valve plate; this means selecting a load for these tests is essential; a desirable load of 20 N, 40 N, 60 N, and 80 N was used in these tests.

This present study focuses on a comparative analysis of the different surface material composition, surface treatment, and material hardness of the valve plate under HM-46 oil lubrication according to load, velocity, temperature, and time on the friction and wear behaviors of the friction pair at low speeds of the swashplate type axial piston pump. Recently, the face of the valve plates and the cylinder block are usually made of different hardness (H.V) materials. As a result, most wear debris deposited on the material has less HV. Copper (usually Brass and red copper) is used for the cylinder block. In contrast, steel, 38CrMoAl, or ductile iron with or without surface coated having different alloy constituents is used for the valve plate. The cylinder block material was B4 brass, which is mainly used to manufacture the cylinder block in swashplate axial piston machines. Therefore, B4 remained constant throughout the tests. The coefficient of friction and wear rate are measured using a ball-on-disc tribometer, and further discussion is made from different results perspectives.

Experimental details

Material selection.

In this study, three different valve plate materials for the axial piston pump machine were supplied by High-Tech Fluid Power Co, Limited (China). They are well known for producing high-standard precision hydraulic pumps. The lower specimens (Valve plate); Cr12MoV Subtract Bronze Coating-chemical vapor deposition (S1), Cr12MOV Subtract Bronze Coating-physical vapor deposition (S2), and ductile Iron (S2), which is without any surface coating. Fig. 2 shows the valve plate with different material compositions.

The upper specimen representing the cylinder block was made of a brass ball (B4). The hardness specimens of which were approximately Vickers Hardness tester was performed using 0.05 kgf load for 10 s, and the average values were obtained by measuring six points on each specimen. Table 1 shows the details of the Vickers hardness for the test

specimens. Moreover, each section of the lower specimens received was cut into equal sizes of 25*20 mm^2. For a better comparison, the contacting surfaces of the lower specimens must have the same surface roughness since the lower specimens are from different pumps having different surface roughness. Therefore, the contacting surfaces were polished mechanically using SIC emery paper with varying grain sizes, from course to optimal fine finish. It should be noted that great care was taken to ensure that the specimens' original surface roughness was as similar as feasible to eliminate any influence on the test results.

The specimens were cleaned with ethanol solution for 5-10 minutes using an ultrasonic cleaner machine, then rinsed with running water and dried well to obtain the optical micrographs and remove any impurity on the surface before and after the tests. H.M. anti-wear hydraulic oil L-HM 46 was used throughout the tests. It has good anti-wear properties, oxidation and foam resistance, and demulsification and rust prevention properties, which are fully compatible with acrylonitrile-butadiene rubber and other sealing materials. Table 2 shows the properties of the oil used for the tests.

The root means square (RMS) value was used to evaluate the surface roughness. The R_a values of the lower specimens were 0.4 µm. The specimens surface topography before coefficient of friction tests is shown in **Error! Reference source not found.**

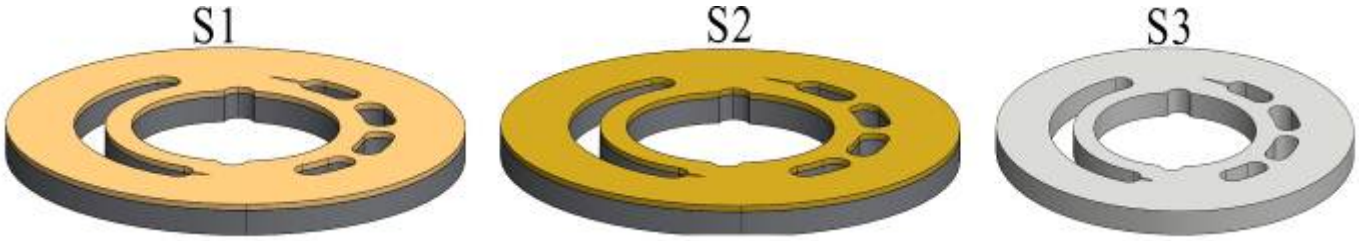

Fig. 2 Friction pair of the valve plate, chemical vapor deposition coating (S1), physical vapor deposition coating (S2), and ductile iron valve plate without surface coating

Table 1 H.V. of specimens under loading force of 0.05 kgf for 10 s

Statistical Results			
Sample Name	**Minimum value**	**Maximum value**	**Average. value**
S1	80.40	96.71	89.38
S2	99.19	171.24	136.30
S2	259.94	282.23	274.94

Table 2 Properties of the hydraulic oil used

L-HM 46 Anti-wear hydraulic oil properties	
Viscosity Index	48.2
Kinematic viscosity (mm^2 /s at 40°C)	96.3
Flashpoint	196
Pour point	-16

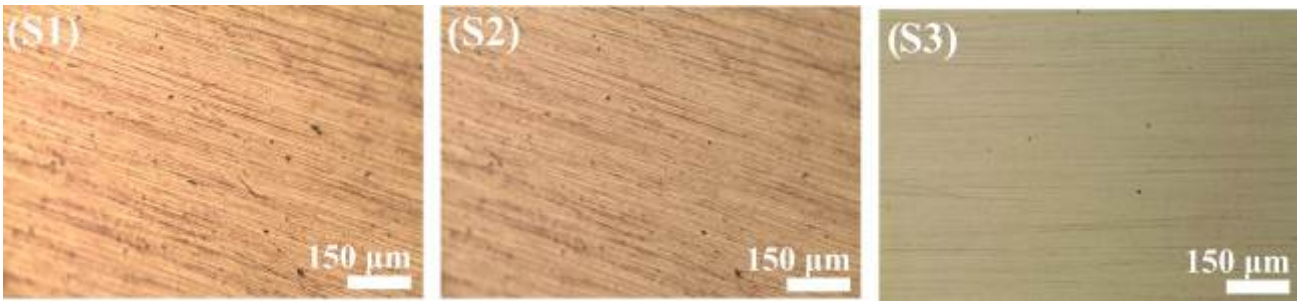

Fig. 3 surface topography of the specimens before the coefficient friction tests

Test Procedure

The coefficient of friction test was performed using HSR-2M high-speed reciprocating friction and wear tester. The reciprocating motion in 5mm stroke length against the upper specimen ball (ϕ6 mm). The rotation speed of the upper specimen was set to 500 rpm throughout the tests. Each test lasts for 20 min with a radius of rotation of 6 mm. The force applied was set to 20 N, 40 N, 60 N, and 80 N. For the level of accuracy, each test was repeated three times for data reproducibility at room temperature between 25 - 27 ℃ with a relative humidity of 40 % -

60%. The matching specimens are shown in the test plan in Table 3. The sections of each wear scar were measured at five different points. The wear volume was calculated on average to reduce the chance of error as in Equation 1. The elementary composition of the specimens is shown in Table 4

The surface topography and morphology were measured using the 3D and profile measurement system equipped with a confocal laser scanning microscope (CLSM), which is featured by acquiring in-focus images from selected depths known as "optical sectioning." An energy dispersive spectrometer (EDS) equipped with a scanning electron microscope (SEM) was also used to identify the surface's chemical elements. SEM images and energy spectrum analysis of the worn surface and debris further speculated the wear mechanism.

$$W.R = \frac{V_l * W_l}{L * S_d} \qquad (I)$$

Where W.R refers to the wear rate; V_l is the volume lost after the test (μm2); W_l is the wear length (m); L is the load force applied (N), and the S_d is the sliding distance of the upper specimen (m).

Table 3 Test conditions for the experiment.

Test condition	Value
Rotation Speed (rpm)	500
Loads (N)	20, 40, 60, 80
Ball diameter (mm)	6
Disc dimension (mm)	25*50
Sidling distance (mm)	5
Lubricant	L-HM 46
The temperature of lubricating oil	29
Lubricant viscosity 40°	96.3
Humidity (%)	40-60

Table 4 Chemical composition of the specimens

Lower specimens (at%)	Cu	Sn	Fe	C	Cr	O	Al	S	Mn
S1	88.6	7.8	1.4		1.8		1.7	0.01	0.1
S2	86	10.5	4.0		1.7		1.7	0.001	0.1
S3			93-94	2.7-2.8	1.4-1.5	0.7	0.8-0.9	0.001	0.001
Upper specimen (at%)	**Cu**	**Zn**	**Pb**	**Cd**	**Hg**	**impurity**			
B4	61.5	balance	<100PPM	<5PM	< 5PPM	<0.0005			

Results and Discussion

Coefficient of friction results

The coefficient of friction (COF) results is summarized in Fig. 4-Fig. 7 for the upper specimen B4 brass sliding on the three lower specimens; S1, S2, and S3, performed under different loading of 20 N, 40 N, 60 N, and 80 N, respectively. When the loading force is large, the ball and the disc are in the sliding friction process, and the contact pressure increases; likewise, the lubrication oil keeps changing. Hence, the gap between the friction pairs varies. The lubrication state is changed from boundary lubrication to mixed lubrication and then to hydrodynamic lubrication since the surface of the specimens is not entirely smooth.

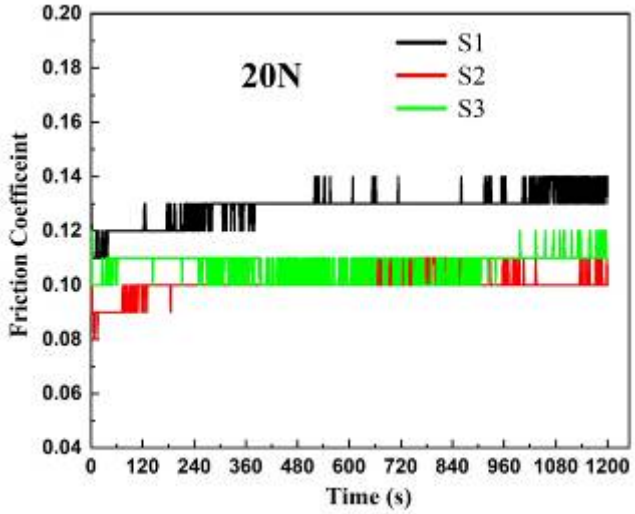

Fig. 4 Measured coefficient of friction during wet reciprocating sliding between B4 and the valve plate materials at a loading force of 20 N

Moreover, from the COF results, most of the debris produced was flushed out of the contact surface, giving a stable coefficient of friction curves for all the applied loads due to the oil used for the lubrication of the interface. The coefficient of friction at 20 N for S1 is slightly higher ~ 0.14 than that of S2 and S2. Even though the difference is slight, the three specimens show very short instability running time due to the effect of the hydraulic oil, and the friction coefficient increased slowly and finally remained stable. The friction coefficient changed slightly with the normal load changing at a constant temperature (Fig. 4-Fig. 7).

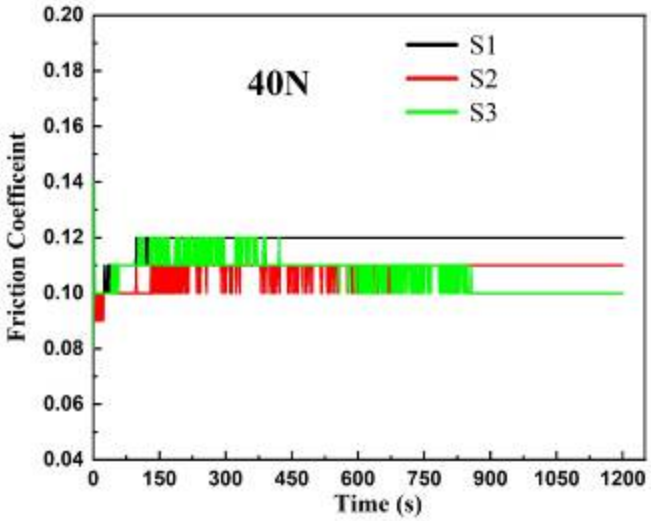

Fig. 5 Measured coefficient of friction during wet reciprocating sliding between B4 and the valve plate materials at a loading force of 40 N

The specimen with bronze layer (S2) could not show a clear dependence on the applied loads and shows consistency in the friction coefficient curves. It can be seen that ductile iron with an uncoated layer could not improve friction compared to coated surfaces S1 and S2. Still, the S1 specimen has the ability to absorb heat from the frictional pair interface when the contact pressure increases (Fig. 4). The bronze layer coating is well-known to increase wear resistance and not purposely for reducing friction [21], [22].

Averagely, from the results of the tribological test shown in (Fig. 4-Fig. 7) for the various test conditions. S2 specimen coating exhibits the lowest coefficient of friction value, and the S1 specimen has the highest COF value. All specimens exhibited similar COF curves, which showed excellent friction-reducing abilities; meanwhile, the addition treated and material composition containing higher Pb element (Table 4) of S2 specimen surface coating showed the best anti-wear abilities.

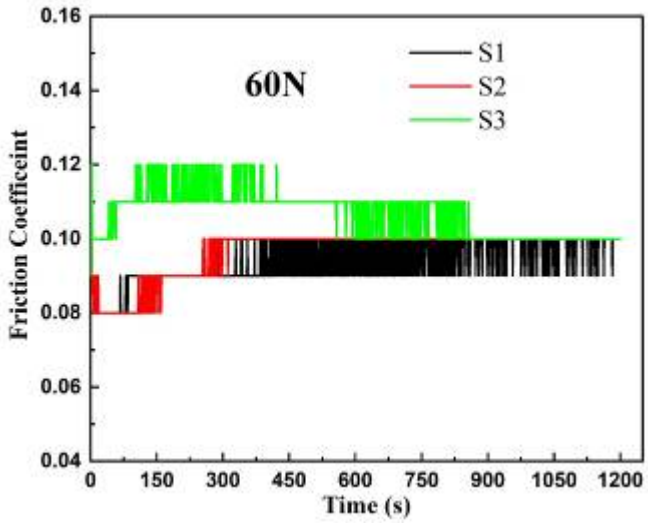

Fig. 6 Measured coefficient of friction during wet reciprocating sliding between B4 and the valve plate materials at a loading force of 60 N

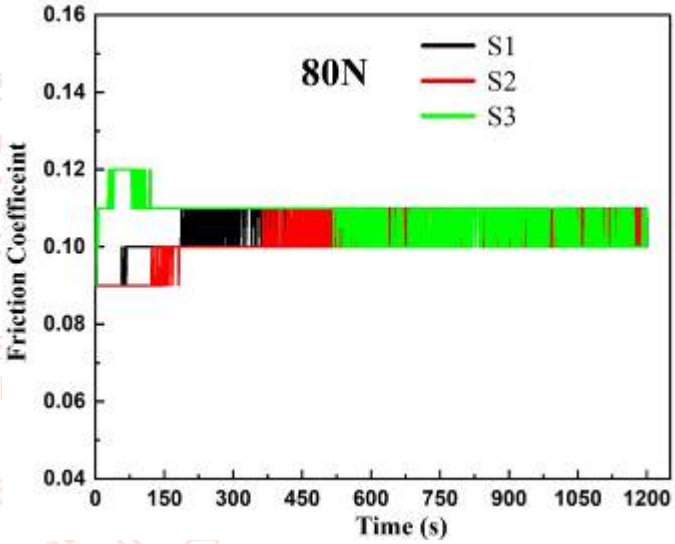

Fig. 7 Measured coefficient of friction during wet reciprocating sliding between B4 and the valve plate materials at a loading force of 80 N

Wear Rate

Ideally, wear that occurs during sliding contact surface is usually considered a mechanical process. However, well-developed models of mechanical wear based on deformation and fracture have been reported [16]. compares the lower specimens' wear rate for the various loading forces applied at a constant temperature. The S3 specimen shows a minimal wear rate (Fig. 8); at the maximum loading force, the wear rate was ~ 1750 um^3/Nm. In other words, the wear resistance of the S3 specimen surface has increased due to the strain hardening of the surface. Hence, it exhibits low wear volume loss and uniform increasing wear rate, rather than a continuous increase of larger volume lost as seen on the S1 and S2 specimens. The wear rates of the S1 specimens are much greater, particularly at 80 N (~10190 um^3/Nm).

Fig. 9 reveals the average wear track of the upper specimen that was used against the lower specimens.

It can be observed that the wear track for S1 and S2 are shallower than those of the S3 specimens. As shown in Fig. 9, the ball for the S3 specimen exhibited larger wear depth, resulting in higher surface deformation as the contact pressure or the loading force increased.

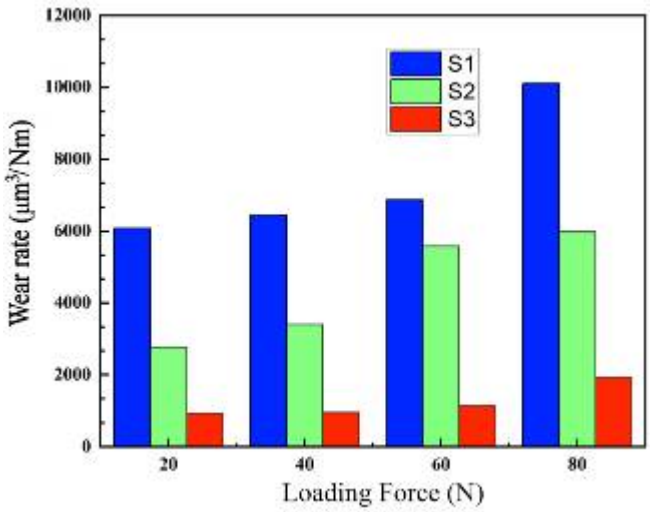

Fig. 8 Average wear rate results of lower specimens for different Loading force

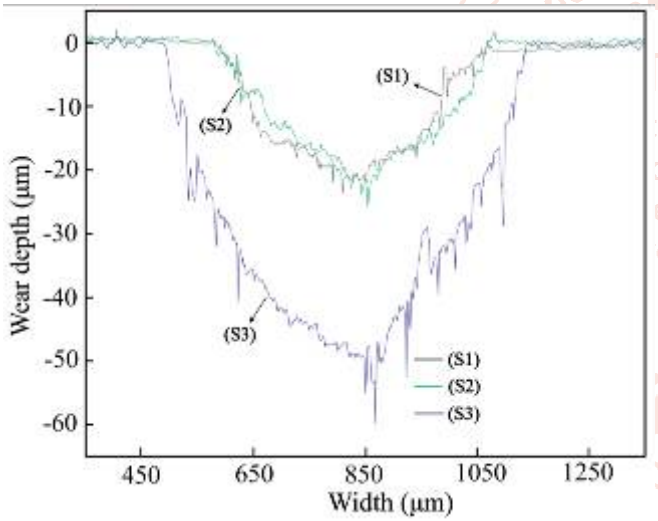

Fig. 9 Profilometry of the average wear tracks of the upper specimen (B4 ball)

These phenomena occurred due to differences in material hardness and strain hardening of the ductile iron surface. As shown in Table 1, the ductile iron hardness is 274.92 HV, whiles the upper specimen (B4) has 168 HV. Therefore, since B4 is softer than ductile iron, the wear and rate of damage occurred more on the B4 (ball) surface as the contact pressure increased.

Wear surface characterization

Fig. 10-Fig. 12 presents the 3D view and SEM images of friction tests generated on wear scar surfaces under different working conditions. The amount of wear debris observed was relatively limited because most debris was flushed out of the wear scar by the lubricating medium, reducing the abrasive wear. Even though ductile iron (S3) had the lowest wear rate (Fig. 8), it caused severe surface deformation to its counter body (Fig. 12), the upper specimen (B4). Many small asperities were found on the surface of the S1 specimen. Abrasive wear, delamination, and spalled surfaces could be present due to the brittleness of the S1 specimen, as exhibited in Fig. 10. These weathered surfaces, representing the third body, are marked by "plowed" tracks generated by debris, in agreement with Fan et al. [23].

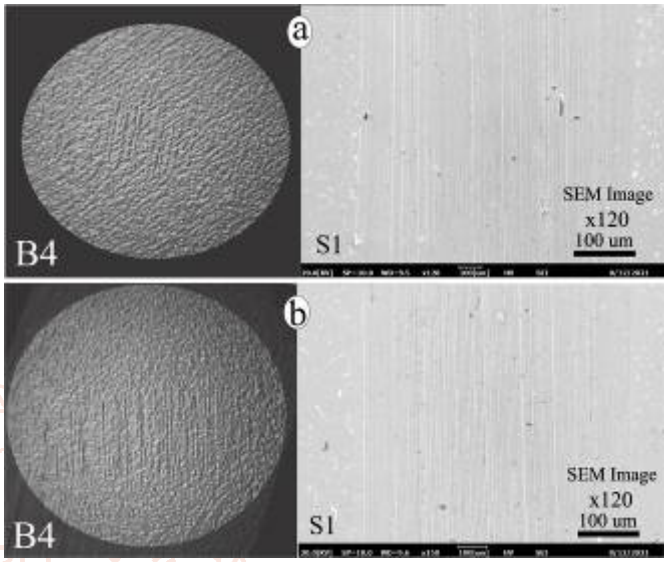

Fig. 10 3D profilometer and SEM images of the surface deformation rate on the upper (B4) and lower (S1) specimens at (a) minimum load of 20 N and (b) maximum load of 80 N

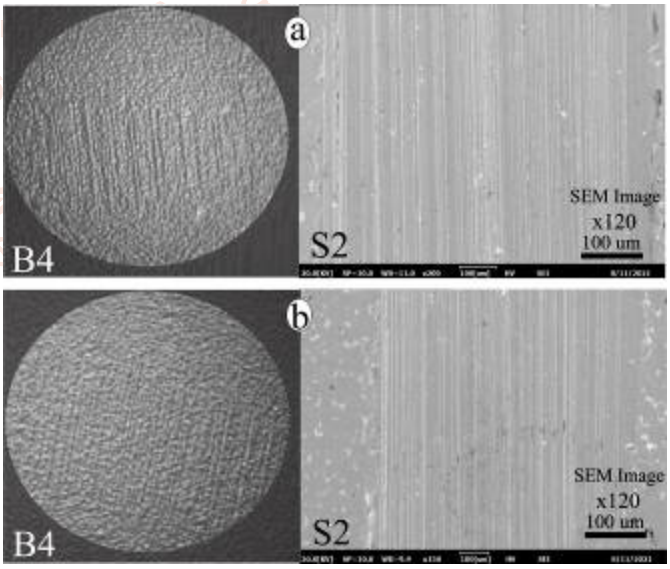

Fig. 11 3D profilometer and SEM images of the surface deformation rate on the upper (B4) and lower (S2) specimens at (a) minimum load of 20 N and (b) maximum load of 80 N, respectively.

As the velocity and loading force increases, more frictional heat is generated, intensifying the plastic deformation of the surface micro protrusions of the bronze coating specimens (S1 and S2). This deformation strengthens the surface hardness of the B4 ball Fig. 10a and Fig. 11a, which improves the wear resistance of the counter surface [24], especially

on the S1 specimen. It ultimately makes the wear surface look smooth (Fig. 11b) at the 80 N loading force. Exfoliate debris was generated under various loads, and flake-like debris was extended with the load increased Fig. 10-Fig. 12 exemplifies that when the load increases (20 N-80 N), the delamination is progressively relieved. Furthermore, the extension of peeling pits is exhibited with the load increasing, suggesting fatigue wear.

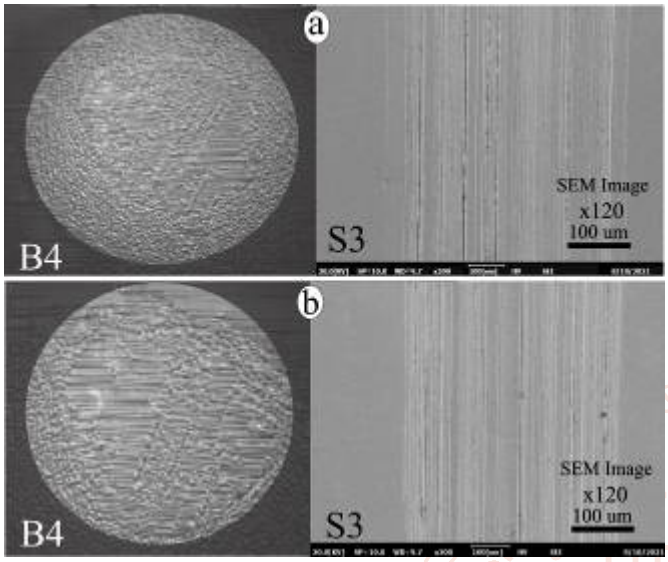

Fig. 12 3D profilometer and SEM images of the surface deformation rate on the upper (B4) and lower (S3) specimens at; (a) minimum load of 20 N and (b) maximum load of 80 N, respectively.

Energy Dispersive Spectra Analysis

The SEM images depict the presence of small particles and some larger particles on the surfaces of the S1 coating. In contrast, S3 has fewer particles than the S2 specimen, with few particles on its surface. The EDS results shown in Fig. 13 further indicated signs of transfer of brass particles. In addition, the presence of Lead (Pb) elements enhances the wear resistance of the surface, the mass fraction of Cu was reduced as the contact pressure increased, and the S1 specimen showed more abrasive grooves at 80 N.

Furthermore, the upper specimen showed few amounts of bronze accumulating on the surface of the B4 due to the influence of the lubricating films and material hardness difference; the EDS analysis Fig. 13-Fig. 14 further confirmed it. Moreso, lead (Pb) elements detected on the surface of the S2 coating were very small for the area analyzed since lead elements are not uniformly distributed on the surface due to their dense nature. As exhibited in Fig. 13, spectrum 3 confirmed the mass fraction loss of Cu on the surface of the S1 specimen.

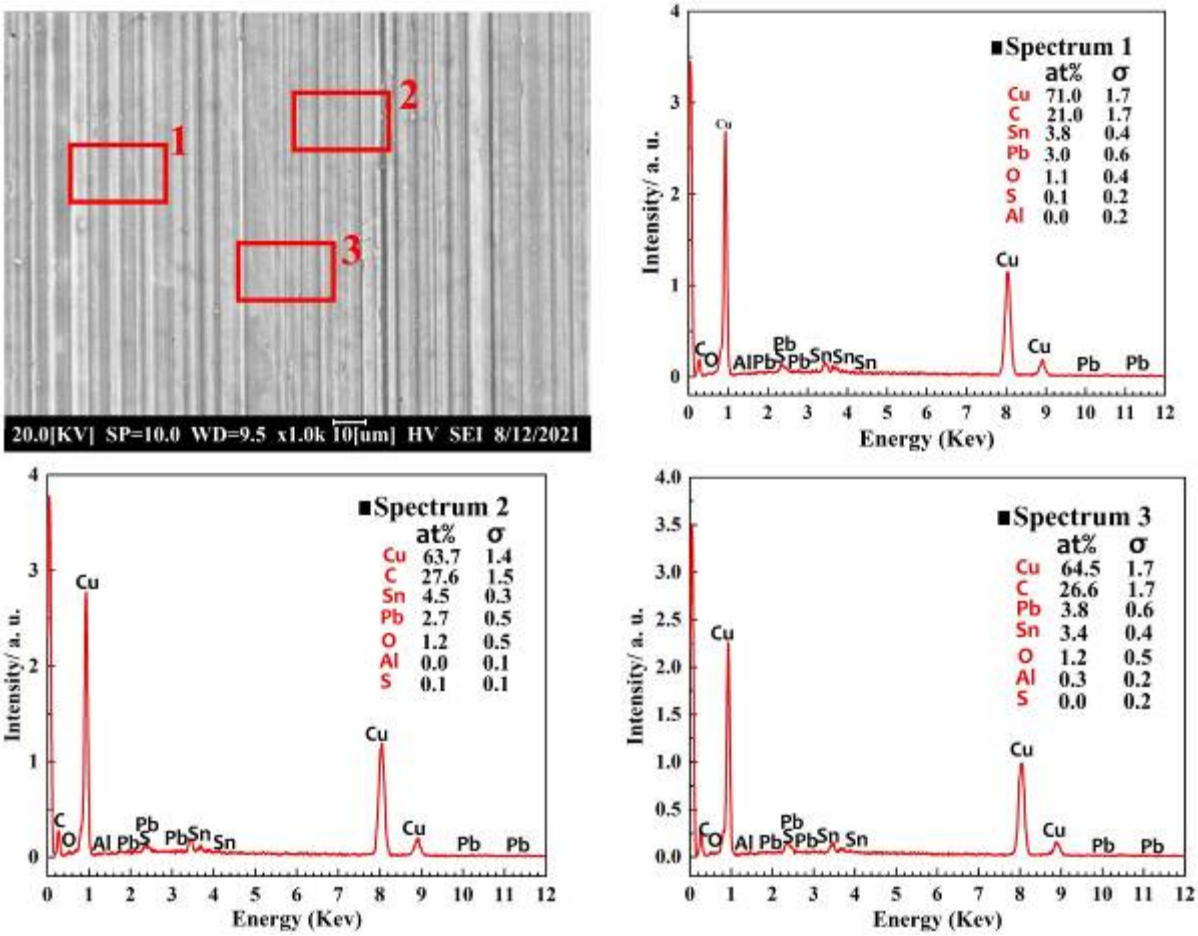

Fig. 13 Energy dispersive X-ray spectrometer (EDS) analysis results for the S1 specimen at 80 N load for three analysis positions with corresponding spectrums.

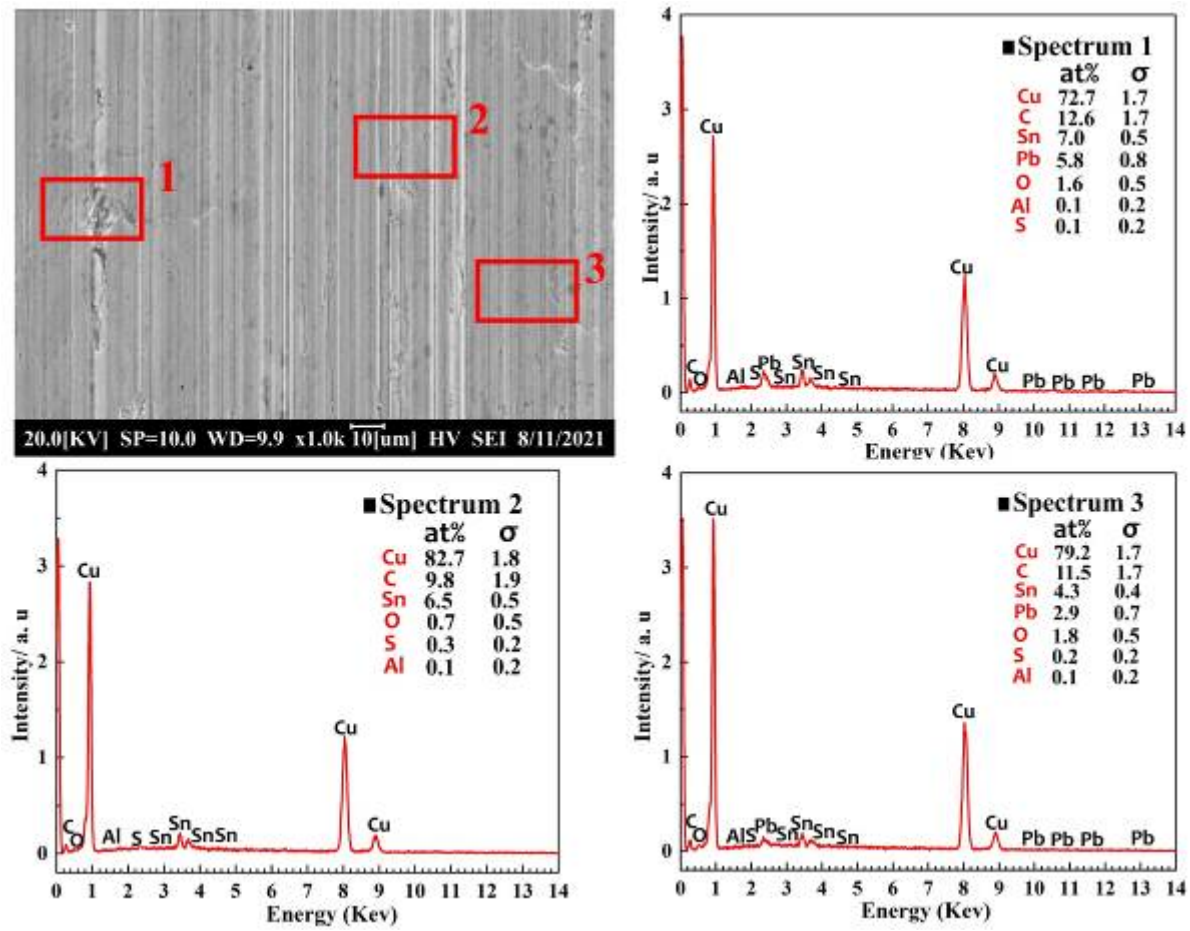

Fig. 14 Energy dispersive X-ray spectrometer (EDS) analysis results for the S2 specimen at 100N load for three analysis positions with corresponding spectra.

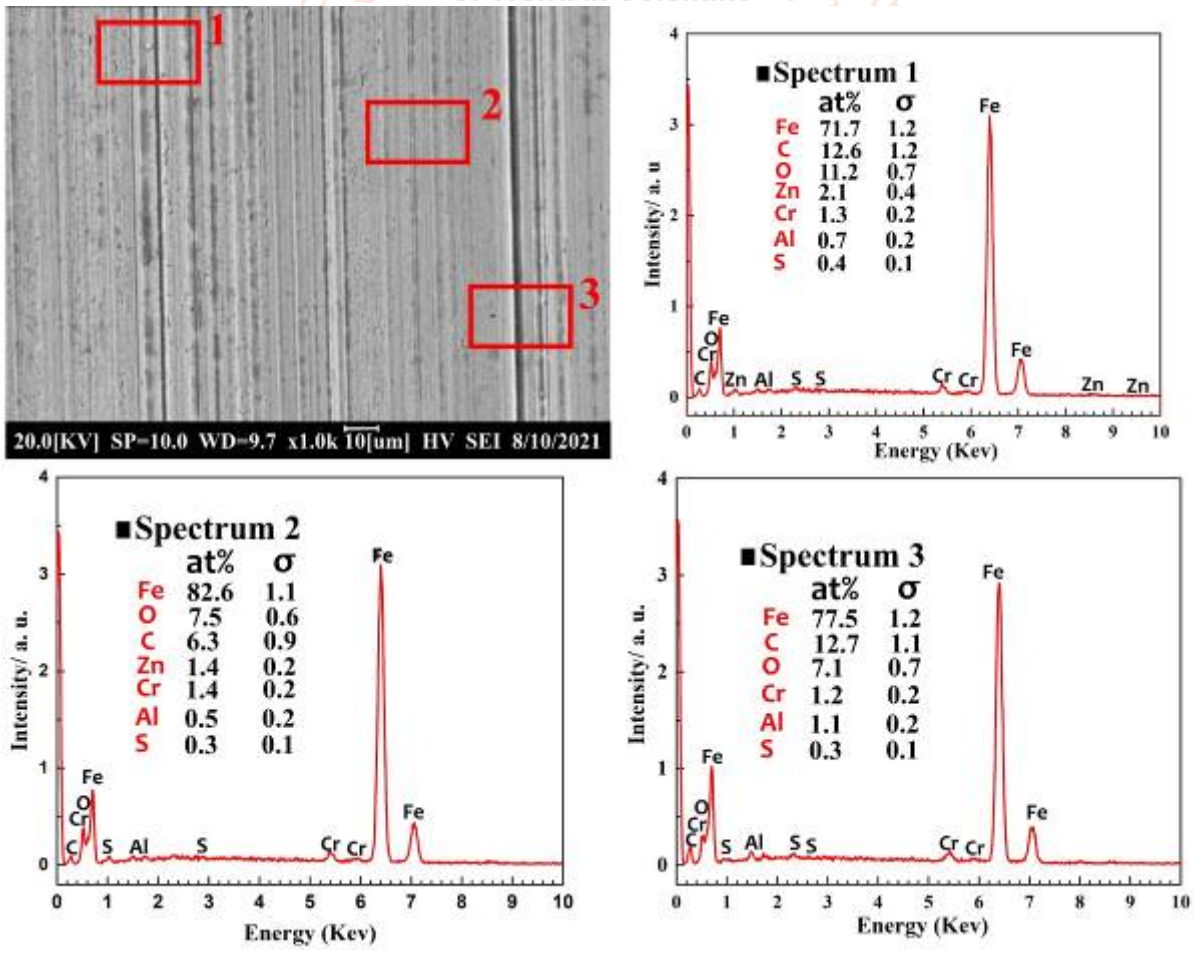

Fig. 15 Energy dispersive X-ray spectrometer (EDS) analysis results for the S3 specimen at 80 N load for three analysis positions with corresponding spectra.

The energy spectrums in Fig. 15 make it evident that the main component of the wear scar is still the original composition of the S2 specimen; there was no possibly material transfer. Even though there were few asperities on

the surface of the ductile iron, it could be observed from Fig. 12 spectrum 3 that the Zn element was detected, which was a transfer from the B4. In addition, the Fe element was reduced dramatically, meaning most of the Fe elements were attached to the surface of the upper specimens in the process of the sliding action.

Additionally, the mass fraction of the O, Al, and s elements gradually increases. Analysis results of the energy spectrums and its mapping of Fig. 12 spectra are exhibited, revealing the dense distribution of O and the bleak S elements. Presumably, the wear process is accompanied by oxidative wear; However, antioxidant elements in ductile iron, such as the Cr and Al, a good anti-oxidation could be possessed [25], inhibiting the occurrence of oxidation reaction to some degree.

Material atomic weight, surface coating, and treatment influence on the friction and wear are remarkable in selecting a valve plate for the swash plate axial piston pump. The choice of material hardness between the specimens (cylinder block/valve interface) dramatically improves the pump's efficiency. On the other hand, Piston pumps are frequently used in harsh conditions. Pumps are difficult to replace during operation; thus, longevity is a significant concern. Although reducing friction lowers the mechanical performance of axial piston pumps and enhances the life span [15], a desirable surface roughness ($R_a \approx 0.4\ \mu m$) is best for this interface since particles are less prone to adhere to smoother surfaces. These particles negatively affect friction and wear. According to the current study, the S2 specimen is a highly recommended surface finish technology for valve plate surfaces under these applied conditions.

Lastly, the above results confirm that the S2 specimen coating provides the lowest friction and optimal wear on both the upper and lower specimens, having fewer asperities and debris on its surface, increasing mechanical efficiency without lowering pump lifetime. It should be emphasized that the contact interface between the valve plate and the cylinder block in this study was simplified to be a ball-on-disc contact. However, the contact condition was set as close to the real scenario as possible.

Conclusion

Based on the findings of orthogonal tests and comparative experiments, the effects of loads on the friction properties and wear mechanism for the three different materials of the valve plate under sliding wear conditions of H.M. 46-oil lubrication were analyzed through graphical representations. The main findings are summarized as follows:

1. When the percentage of Pb in the material increases, the friction, and wear rate coefficient first decreases before rising again as the loading force increases. On the S2 specimen, 10 wt% Pb content compare to the other specimens, solid lubricant coating forms, leading to the minimal wear rate and surface deformation.

2. Although the ductile iron-type valve plate showed better wear resistance than the other two specimens, it causes more damage to the ball surface (cylinder block), increasing the wear rate for the cylinder block. In this regard, in selecting materials for the cylinder block/valve plate interface, the differences in the material hardness must be considered, as 38CrMoAl substrate bronze coating shows optimal COF, wear rate, and asperities' transfer on the surfaces of the upper and lower specimens.

3. Therefore, this study reveals that 38CrMoAl substrate bronze coating is best for fabricating the valve plate in a swashplate axial piston pump at low-speed operation. An important caveat of this research is that the contact interface between the valve plate and the cylinder block was simplified to a ball-on-disc interaction. Still, we aimed to make the contact condition as realistic as feasible.

Acknowledgment

The authors would like to thank Dr. Geoffrey Micah Bentum, Dr. Moses A. Ameyaw, Eva Akwer, Terrence Thomas Tetteh, and the rest of the research team for their hard work in this study's success.

References

[1] T. Kazama, H. Sasaki, and Y. Narita, "Simultaneous temperature measurements of bearing and seal parts of a swash plate type axial piston pump - effects of piston clearance and fluid property," J. Mech. Sci. Technol., vol. 24, no. 1, pp. 203–206, 2010, doi:10.1007/s12206-009-1162-1.

[2] Y. Li, Z. Ji, L. Yang, P. Zhang, B. Xu, and J. Zhang, "Thermal-fluid-structure coupling analysis for valve plate friction pair of axial piston pump in electrohydrostatic actuator (EHA) of aircraft," Appl. Math. Model., vol. 47, pp. 839–858, Jul. 2017, doi:10.1016/j.apm.2016.08.015.

[3] T. Zloto and P. Stryjewski, "Modeling the Load of the Kinematic Pair Piston-cylinder in an Axial Piston Pump by Means of FEA," Procedia Eng., vol. 177, pp. 233–240, 2017, doi: 10.1016/j.proeng.2017.02.194.

[4] J. Zhao, Y. Fu, J. Ma, J. Fu, Q. Chao, and Y. Wang, "Review of cylinder block/valve plate interface in axial piston pumps: Theoretical models, experimental investigations, and optimal design," Chin. J. Aeronaut., vol. 34, no. 1, pp. 111–134, Jan. 2021, doi:10.1016/j.cja.2020.09.030.

[5] J. Ki Kim and J.-Y. Jung, "Measurement of fluid film thickness on the valve plate in oil hydraulic axial piston pumps (I)-bearing pad effects-," KSME Int. J., vol. 17, no. 2, pp. 246–253, Feb. 2003, doi: 10.1007/BF02984396.

[6] I. S. Cho, "A study on the optimum design for the valve plate of a swash plate-type oil hydraulic piston pump," J. Mech. Sci. Technol., vol. 29, no. 6, pp. 2409–2413, Jun. 2015, doi:10.1007/s12206-015-0533-z.

[7] J. Zhang et al., "Simulation and experimental investigation on low wear rate surface contour of piston/cylinder pair in an axial piston pump," Tribol. Int., vol. 162, p. 107127, Oct. 2021, doi:10.1016/j.triboint.2021.107127.

[8] G. Wan, Q. Wu, X. Yan, and K. Yang, "Tribological properties of the plate valve and rotor material of hydraulic vane motor on different ambient temperature," Wear, vol. 426–427, pp. 887–895, Apr. 2019, doi:10.1016/j.wear.2019.01.075.

[9] M. Pelosi and M. Ivantysynova, "The Impact of Axial Piston Machines Mechanical Parts Constraint Conditions on The Thermo-Elastohydrodynamic Lubrication Analysis of The Fluid Film Interfaces," Int. J. Fluid Power, vol. 14, no. 3, pp. 35–51, Nov. 2013, doi:10.1080/14399776.2013.10801412.

[10] S. Y. Lee, S. D. Kim, and Y. S. Hong, "Application of the duplex TiN coatings to improve the tribological properties of Electro Hydrostatic Actuator pump parts," Surf. Coat. Technol., vol. 193, no. 1-3 SPEC. ISS., pp. 266–271, 2005, doi:10.1016/j.surfcoat.2004.07.053.

[11] Y. S. Hong and S. Y. Lee, "A comparative study of Cr-X-N (X=Zr, Si) coatings for the improvement of the low-speed torque efficiency of a hydraulic piston pump," Met. Mater. Int., vol. 14, no. 1, pp. 33–40, Feb. 2008, doi: 10.3365/met.mat.2008.02.033.

[12] Y. Hong, S. Lee, S. Kim, H. L.-J. of mechanical science And, and U. 2006, "Improvement of the low-speed friction characteristics of a hydraulic piston pump by PVD-coating of TiN," Springer.

[13] P. W. Michael, J. M. Garcia, S. S. Bair, M. T. Devlin, and A. Martini, "Lubricant Chemistry and Rheology Effects on Hydraulic Motor Starting Efficiency," Tribol. Trans., vol. 55, no. 5, pp. 549–557, Sep. 2012, doi:10.1080/10402004.2012.680208.

[14] Y. Zhu, X. Chen, J. Zou, and H. Yang, "A study on the influence of surface topography on the low-speed tribological performance of port plates in axial piston pumps," Wear, vol. 338–339, pp. 406–417, Sep. 2015, doi:10.1016/j.wear.2015.07.016.

[15] Y. Zhu, X. Chen, J. Zou, and H. Yang, "A study on the influence of surface topography on the low-speed tribological performance of port plates in axial piston pumps," Wear, vol. 338–339, pp. 406–417, 2015, doi:10.1016/j.wear.2015.07.016.

[16] U. Olofsson and S. Dizdar, "Surface analysis of boundary-lubricated spherical roller thrust bearings," Wear, vol. 215, no. 1, pp. 156–164, Mar. 1998, doi: 10.1016/S0043-1648(97)00259-7.

[17] E. Bergseth, S. Sjöberg, and S. Björklund, "Influence of real surface topography on the contact area ratio in differently manufactured spur gears," Tribol. Int., vol. 56, pp. 72–80, Dec. 2012, doi: 10.1016/j.triboint.2012.06.014.

[18] A. Yamaguchi, "Formation of a Fluid Film between a Valve Plate and a Cylinder Block of Piston Pumps and Motors : 2nd Report, A Valve Plate with Hydrostatic Pads : Heat Transfer, Combustion, Power, Thermophysical Properties," JSME Int. J., vol. 30, no. 259, pp. 87–92, 1987, doi: 10.1299/jsme1987.30.87.

[19] C. Zhang, S. Wang, M. Tomovic, and L. Han, "Performance Degradation Analysis of Aviation Hydraulic Piston Pump Based on Mixed Wear Theory," Tribol. Ind., vol. 39, no. 2, pp. 248–254, Jun. 2017, doi:10.24874/ti.2017.39.02.12.

[20] Z. Wang, S. Hu, H. Ji, Z. Wang, and X. Liu, "Analysis of lubricating characteristics of valve plate pair of a piston pump," Tribol. Int., vol.

126, pp. 49–64, Oct. 2018, doi:10.1016/j.triboint.2018.05.008.

[21] W.-Y. Li, C.-J. Li, H. Liao, and C. Coddet, "Effect of heat treatment on the microstructure and microhardness of cold-sprayed tin bronze coating," Appl. Surf. Sci., vol. 253, no. 14, pp. 5967–5971, May 2007, doi:10.1016/j.apsusc.2006.12.108.

[22] Q. Luo, Z. Wu, Z. Qin, L. Liu, and W. Hu, "Surface modification of nickel-aluminum bronze alloy with gradient Ni-Cu solid solution coating via thermal diffusion," Surf. Coat. Technol., vol. 309, pp. 106–113, Jan. 2017, doi:10.1016/j.surfcoat.2016.11.013.

[23] H. H. Nguyen, S. Wan, K. A. Tieu, S. T. Pham, and H. Zhu, "Tribological behaviour of enamel coatings," Wear, vol. 426–427, pp. 319–329, Apr. 2019, doi: 10.1016/j.wear.2019.02.002.

[24] H. Yan and Z. Wang, "Effect of heat treatment on wear properties of extruded AZ91 alloy treated with yttrium," J. Rare Earths, vol. 34, no. 3, pp. 308–314, Mar. 2016, doi:10.1016/S1002-0721(16)60030-3.

[25] C. M. Liu, H. M. Wang, S. Q. Zhang, H. B. Tang, and A. L. Zhang, "Microstructure and oxidation behavior of new refractory high entropy alloys," J. Alloys Compd., vol. 583, pp. 162–169, Jan. 2014, doi:10.1016/j.jallcom.2013.08.102.